https://doi.org/10.3311/PPci.19141

Periodica Polytechnica Civil Engineering, 66(2), pp. 653–669, 2022

Particle Size Effect on DEM Simulation of Pressures Applied on a Cylindrical Silo with Hopper

Sami Houhamdi[1*], Eutiquio Gallego Vazquez[2], Kamel Djeghaba[1]

[1] Civil Engineering Laboratory - LGC, University Badji Mokhtar of Annaba, BP 12, 23100 Annaba, Algeria
[2] Department of Agricultural Engineering, BIPREE Research Group, ETSI Agronomica, Alimentaria y de Biosistemas, Universidad Politecnica de Madrid, 28040 Madrid, Spain
* Corresponding author, e-mail: sami.houhamdi@univ-annaba.org

Received: 24 August 2021, Accepted: 15 March 2022, Published online: 25 March 2022

Abstract

This work is a contribution to the comprehension of the particle upscaling effect on DEM simulation of cylindrical silos. Three silo models have been simulated with different hopper outlets and inclination angles. Huge calculations of 11 simulation series with a different scaling factor are considered for every model. Pressures applied on silo walls remain quite identical with particle upscaling. Besides, their curves are in agreement with Eurocode standard. The computing time is significantly reduced as well as the number of particles, where the simulation speed is increased up to 12 times by just scaling particle radius two times. The total bulk density was not affected by particle escalation and its value remains unchanged.

Keywords

DEM simulation, steel silo, particle upscaling, coarse graining, pressure, granular material flow

1 Introduction

Discrete element method (DEM) is a part of the numerical methods family that allowed to simulate the motion of a large number of particles. This method is based essentially on Newton's second law of motion to simulate individually each particle of the system. At a given time step, this method is checking the position of every particle, in order to detect particle-to-particle and particle-to-wall contacts. The contact is determined if there is an overlap between elements. Depending on the amount of overlap, the impact force is calculated, which determines the new velocity and direction of the particle. The incremental time step has to be small enough to avoid problems such as excessive particle overlapping, high particle velocities, or large contact forces. Time step in DEM simulations is usually calculated as a fraction of the critical Rayleigh's time, with frequent values in the range of 10%~40% of Rayleigh's time step [1].

Today, DEM is well recognized as an approved method and a very effective tool for solving engineering problems in granular materials, especially particles flow [2–6]. Silos are widely used structures to storage various granular materials, which have complex behavior that is commonly simulated by using DEM [7, 8]. Unfortunately, this method has limitations due to the computing power where some cases require a non-reasonable calculation time. Even with advanced technologies, such as parallel processing and Graphics Processing Units (GPUs), the simulation of a large number of particles in full-scale applications is still impossible. Computational time greatly increases with irregular particle shapes, particle stiffness [4], and especially large containers with a high number of particles. Because of this problem, many alternative procedures have been used to reduce the real computational time required by a DEM model, e.g., the use of 2D models instead of real 3D simulations [9], periodic boundary conditions applied to simulate only a slice of the silo [10], or using small container dimensions [6]. Some other simplifications are based on particle shape and properties. The multi-spheres method is used to model a complex particle in order to obtain an approximate equivalent volume and shape. The reduction of the number of spheres leads to reduce the calculation time [11]. By reducing the Young modulus, the critical time step reduces as well [12], which is one of the targeted criteria for less computing time.

The reduction in the number of particles considered in the simulation would be the most effective procedure to decrease the computing time required to analyze a large silo.

Cite this article as: Houhamdi, S., Vazquez, E. G., Djeghaba, K. "Particle Size Effect on DEM Simulation of Pressures Applied on a Cylindrical Silo with Hopper", Periodica Polytechnica Civil Engineering, 66(2), pp. 653–669, 2022. https://doi.org/10.3311/PPci.19141

For this purpose, several approaches have been created based on scaling up the size of particles. The "Exact Scaling" [13, 14] is the most accurate scaling approach but it doesn't help to reduce the computing time or the number of particles. Its aim is to simulate the same behavior of the original problem in larger or smaller size by scaling the particle size and the geometry dimensions with the same factor. Another approach called "Scalping" or "Cut off" [15], provides for scaling the particle size in a specific region with keeping the same geometry dimensions, the finer particles in the selected region are replaced by bigger particles. The "Coarse-Graining" or "Upscaling" is the most effective approach to reduce the computing time by scaling up the size of all particles while maintaining the same geometry and domain dimensions [16–22]. The bigger size leads to reduce the total number of particles, also this technique helps to increase the critical time step. The effects of this approach have been studied by many authors and their results are conflicting and not conclusive. Grima and Wypych [23] have simulated a belt conveyor and the impact force on a flat plate. The results show that scaling the particle size by 23% has no significant influence on the impact force. However, by using a scale factor of 2 to 3 the result is not consistent between the simulations and the impact force is greatly deviating. Also, they found that the modification of the contact stiffness and the coefficient of restitution are negligible. Xie et al. [24] have studied the particle size effect on the behavior of granular flow transportation in conveyor transfer by changing the diameter scale and keeping the other parameters as the unscaled case. They found that the flow behavior did not influence by a scaling factor of 2 but the impact force is higher than the experimental results. Achmus and Abdel-Rahman [25] found a remarkable particle scale effect and a new calibration must be performed if the scaling factor has been changed. By scaling the particle size, the density is conserved and the scaled model should have the same energy as the unscaled model [26]. According to [18], by keeping the same Young's modulus, the contact stiffness and damping of the coarse model are the same as the original model. Roessler and Katterfeld [22] have discussed the scalability of the angle of repose test using a lifting cylinder, they concluded that the cylinder diameter does not influence the angle of repose. Also, by scaling both particle size and cylinder size, the coefficient of friction is the same as the original and there is no significant effect on the angle of repose result. They recommended using the friction coefficient obtained from the unscaled particle for the scaled particle in the industrial simulation. Coetzee [17] has successfully calibrated upscaled particles and he concluded that the hopper discharge rate and the velocity field can be accurately predicted by using a scale factor of 1.3 with an error of less than 10%. Weinhart et al. [27] investigate the influence of coarse-graining and micro-macro transition, they show that this technique provides meaningful results.

The effects of particle upscaling without changing its parameters or shape are investigated in this paper as a contribution for more understanding of this technique, especially for the cylindrical silos with different hopper types and flow patterns. The results are obtained for three different silo models, every model has a different hopper inclination or outlet size. Particle upscaling is applied by scale the radius with a factor up to 3.0 with an increment of 0.2 (11 different scales including the unscaled model). The aim is to conclude these effects on the pressures exerted over the silo walls by taking into account the hopper type.

2 Materials and methods

The research work accomplished in this paper was the comparison of results obtained with DEM simulations for filling and emptying of a cylindrical silo when using the unscaled models, with other simulations made by using the upscaling technique. The size of particles considered in all simulations is calculated by using a scale factor varying from 1.0 to 3.0.

2.1 Discrete Element Method

DEM is mainly based on an approximate solution of motion equation by assuming that the velocity and the acceleration are constant during the time step. Particles are mostly rigid in some fields, whereas in others, such as rock mechanics, deformable elements are used. The deformation can be determined through the amount of the overlap between the particles in contact. The interaction between particles determines the resultant forces on each particle. The new velocity and acceleration are obtained by applying Newton's second law of motion. The new equation of motion is numerically integrated to obtain displacement and a new position. This process repeats every time step for each particle in the system [28].

2.1.1 Time step

The amount of time between iterations is defined as "Time Step", which is typically chosen as a percentage of the Raleigh Time Step. Higher particle energy in the system (appears as higher forces and faster collisions) requires

a lower time-step value. The small time step significantly increases the computational time with more details of the results. Conversely, a large time step reduces computational time but may cause particles to behave erratically [1].

2.1.2 Time integration scheme

Solving the equation of motion is the most important part of DEM simulation. The time integration scheme used to solve this equation is the key to numerical stability.

Time integration methods can be broadly classified into two categories, implicit and explicit methods. Choosing one of them is based on their computational characteristics, stability, and accuracy. The appropriate integration scheme allows choosing larger time steps. In this case, the simulations can be significantly speed up. Implicit methods usually solve nonlinear equations that require a series of iterations at each time step resulting in much more computing time compared to explicit methods. However, these methods can unconditionally reach stability in linear analysis with high precision. On the other hand, the explicit methods solve the equations directly after one iteration. The computational effort per time step is low in this case but the stability criteria should be achieved. Thus, a small time step is required [29].

2.1.3 Contact parameters

Contact parameters used in the present work are three coefficients: restitution, static friction, and rolling friction. Restitution coefficient is the ratio between the initial relative velocity (before collision) and rebound relative velocity (after collision). The normal range is between 0 and 1 where a value of 0 is a perfectly inelastic collision while a value of 1 indicates a perfectly elastic collision. The ratio of the static friction force to the normal force is defined as the static friction coefficient. The coefficient of rolling friction represents the amount of torque required to transmit motion to an object resting on a flat surface. It is defined as the ratio of the rolling friction force (rolling resistance) to the normal force [30].

2.2 Silo geometry

In order to compare the effect of particles escalation on different hopper types and outlet sizes, we used three silo models, model A, model B, and model C (Fig. 1). All models have a cylindrical shape with the same bin dimensions, which are 200 mm for the diameter, and 250 mm for the bin height, thus showing an aspect ratio h_c/d_c = 1.25. According to EN 1991-4, all models are classified as an intermediate slenderness silo. Model A and model B have the same hopper height (100 mm), whereas different outlet diameters are used (80 mm and 60 mm, respectively). Similar to model B, an outlet diameter of 60 mm is used for model C, while the hopper height is different (50 mm). Model A and model B would have a steep hopper type, while model C has a shallow hopper [31].

2.3 Material

All simulations are performed by using dry wheat material. The multi-sphere method is used to simulate the particle shape with three spheres as an approximation of the

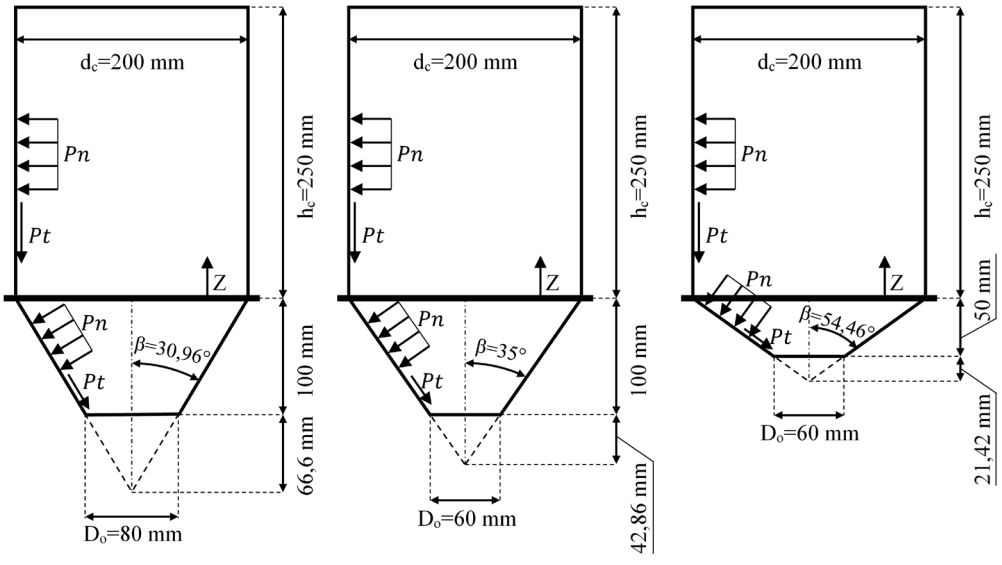

Fig. 1 Dimensions of the three silo models used in the simulation

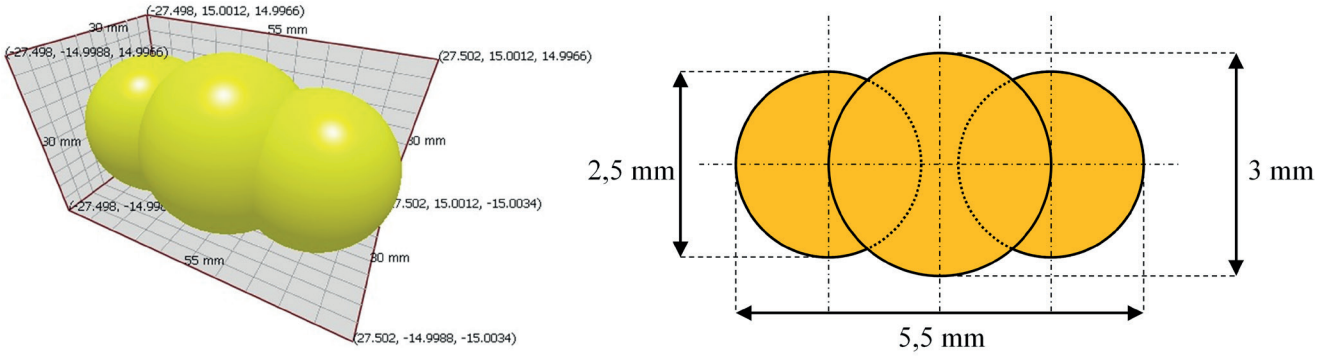

Fig. 2 Particle shape and dimensions

real grain shape (shown in Fig. 2). The distance between every sphere center is 1.5 mm, while they have diameters of 2.5 mm, 3.0 mm, and 2.5 mm, respectively [32]. The shape of particles used can influence on many aspects of the friction effects between the material and walls, or the mass flow rate, and could be further considered in additional research. However, the authors have limited in this paper to the shape.

Table 1 shows the mechanical properties of the wheat particle, whose values were adopted from [33]. In addition, the usually employed mechanical properties for steel are defined in Table 1. The Hertz-Mindlin contact model was considered for particle-to-particle and particle-to-wall contacts, assuming viscous damping in the normal and tangential directions, and frictional damping in the tangential direction. The simulation of this contact model requires the definition of three parameters of interaction between wheat particles and silo steel walls: the coefficient of restitution G_r, the coefficient of static friction μ_0, and the coefficient of rolling friction f, whose values can be found in Table 1 [33].

2.4 Simulation process

EDEM Academic 2018.2 [1] is used to perform all simulations. The simulation process is divided into three phases, the filling phase, the rest phase, and the emptying phase.

Table 1 Mechanical parameters used in the DEM models

Parameter	Wheat	Steel
Poisson ration v	0.4	0.3
Density ρ (kg/m^3)	1430	7500
Shear modulus G (Pa)	3.58×10^8	8×10^{10}
Coefficient of restitution G_r	Wheat: 0.5	Wheat: 0.6
	Steel: 0.6	/
Coefficient of static friction μ_0	Wheat: 0.3	Wheat: 0.25
	Steel: 0.25	/
Coefficient of rolling friction f	Wheat: 0.01	Wheat: 0.01
	Steel: 0.01	/

For the first phase, the progressive filling method is used with a cylindrical particles generator situated at the top center of the silo, where it is considered as a central filling. Without initial velocity, all particles are generated in random positions and orientations inside the generator, taking into consideration 2 kg/sec as particle generation rate. The generated particles started falling under gravity force until the silo was filled (Fig. 3). Once the silo is completely filled, the particle generator is removed and the simulation has continued until the static state is reached (the rest phase), which is assumed to occur when the kinetic energy at that moment is constant with a negligible value (varying depending on the model, but lower than 1e-8 in all models) and the coordination number and number of contacts remain constant. The emptying of the silo is the final phase, which starts by removing the outlet surface allowing particles to flow out of the silo until it was completely emptied.

The non-spherical shape of the adopted particle makes the comparison of models difficult when scaling the particle size. Because of this, the equivalent radius, R_{eq}, was calculated as the radius of a "virtual" spherical particle whose volume, V, would be the same as the simulated particle (Eq. (1)). Thus, the previously simulated wheat particle has a total volume of 24.88 mm^3, then resulting in an equivalent radius of 1.81 mm. The radius scaling factor, f_R, is defined as the ratio between the equivalent radius, which corresponds to the scaled particle, $R_{eq,s}$, and the equivalent radius obtained for the original simulated particle size, $R_{eq,0}$ (Eq. (2)). It is obvious that the value corresponding to $R_{eq,0}$ can be found in Table 2 for a radius scaling factor equals 1.0.

For more understanding of particle upscaling effect on the results, 11 radius scale factors f_R are considered, starting from 1.0, which corresponds to the real size, until f_R of 3.0 with incremental steps of 0.2. The particle scaling factor was limited to this maximum value in order to avoid the appearance of blockages at outlet during the emptying

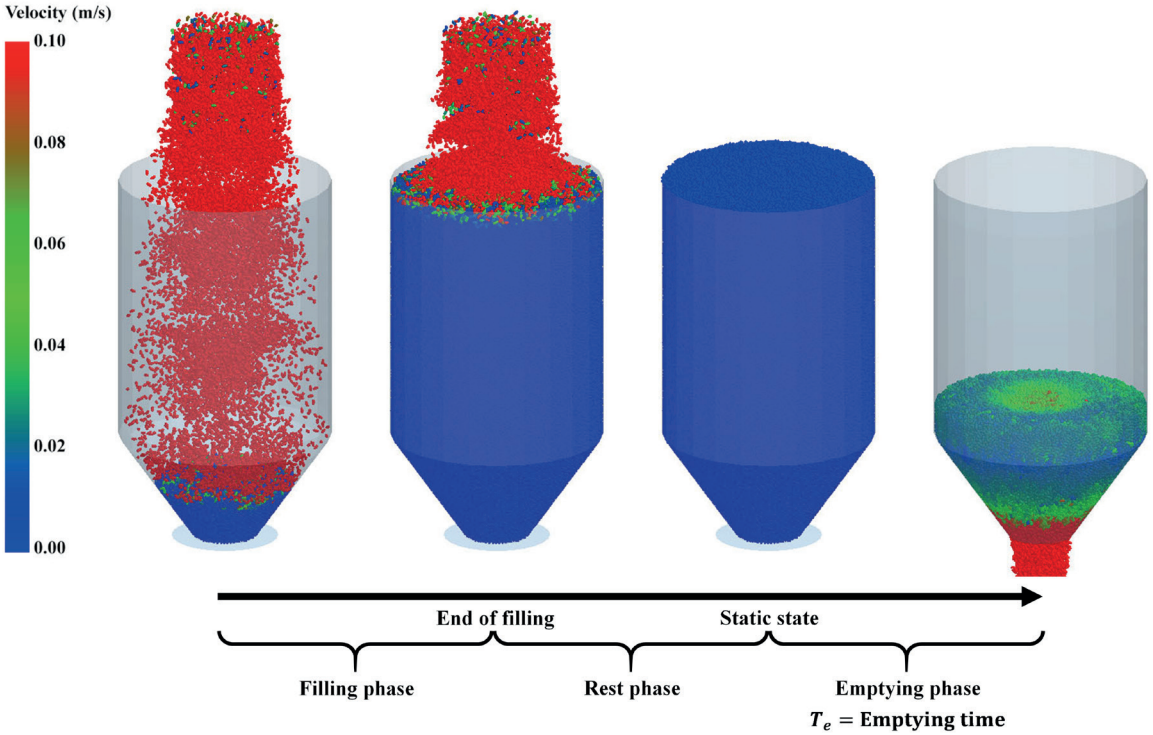

Fig. 3 Progressive filling and emptying of the silo

Table 2 Parameters affected by radius escalation

f_R: Radius scaling factor		1.0	1.2	1.4	1.6	1.8	2.0	2.2	2.4	2.6	2.8	3.0
R_{eq}: equivalent radius of the particle (mm)		1.81	2.17	2.54	2.90	3.26	3.62	3.98	4.35	4.71	5.07	5.43
(D_o/D_{eq})	D_o = 80 mm	22.09	18.41	15.78	13.81	12.27	11.04	10.04	9.20	8.50	7.89	7.36
	D_o = 60 mm	16.57	13.81	11.83	10.35	9.20	8.28	7.53	6.90	6.37	5.92	5.52
V: volume of particle (mm^3)		24.88	42.99	68.26	101.89	145.08	199.01	264.89	343.9	437.23	546.09	671.67
m: mass of particle (kg × 10^{-3})		0.0356	0.0615	0.0976	0.1457	0.2075	0.2846	0.3788	0.4918	0.6252	0.7809	0.9605
Rayleigh's time step (s × 10^{-6})		8.333	10	11.666	13.333	15	16.666	18.333	20	21.666	23.333	25

phase. Particle escalation directly affects several properties such as particle volume, mass, equivalent radius (R_{eq}), and Rayleigh's time (Table 2).

$$R_{eq} = \sqrt[3]{\frac{3V}{4\pi}} \tag{1}$$

$$f_R = \frac{R_{eq,s}}{R_{eq,0}} \tag{2}$$

Particle escalation was performed by multiplying each sphere radius, as well as the distance between the spheres, by the scaling factor considered (all length dimensions are scaled in direct proportion to the scale factor). For the scaled particle, the original volume and mass are multiplied by the cube of the radius scale factor (or by the volume scale factor). In this case, the volume and the total mass are conserved, since the scaled particle has the same volume and mass as its representative group of the unscaled particles. The moment of inertia is also corrected based on the scaled particle model.

In addition, the ratio between the outlet diameter, D_o, and the equivalent diameter of the scaled particle, D_{eq}, was obtained for each simulation (Table 2). The time step used in the simulations is 30% of Rayleigh's time with a saving interval of 0.01 s. This Rayleigh's time was selected because of the low overall energy in the system and the reduced velocities that most of the particles exhibited during the simulation. So, the adopted time step would reduce the number of iterations required per second, then reducing the total computational time required. This is especially important for those models having the largest number of particles. However, the time step considered in the simulations was always lower than 10^{-6}, and it was checked that results had an adequate stability.

2.5 Method of obtaining pressures

The vertical distributions of normal, (*Pn*), and tangential pressures, (*Pt*), are one of the main results studied in the present work. The silo bin mesh is vertically divided into 11 areas to get more accurate results. Every area (*Av*) has a height of 25 mm except the two areas above the transition zone where their height is 12.5 mm. The vertical divisions of hopper mesh are 10 for models A and B with a height of 10 mm for each area, while the hopper of model C has 8 divisions of 6.25 mm height for each. The radial divisions are 24 for all models where every division (*Ar*) contains a pair of triangular mesh areas (Fig. 4).

The pressures were evaluated using the vector of total forces that act on every radial mesh area *Ar*, where the forces are generated with every contact between particles and silo walls. The normal force $Fn_{i,j}$ and tangential force $Ft_{i,j}$ are the projections of force vector components on radial area number *j* from vertical area number *i* ($Ar_{i,j}$), in normal and tangential directions, respectively. Fn_i is the sum of normal forces applied to radial areas of the vertical area *i* (Eq. (3)), as well as Ft_i which is the sum of tangential forces applied to the same radial areas (Eq. (4)). The normal and tangential pressures exerted on every vertical area *i* were evaluated as the maximum values over time, which are obtained using Eq. (5) and Eq. (6), respectively, for filling and emptying cases. The mobilized friction obtained by DEM, $\mu_{w,\mathrm{DEM}}$, is the ratio of tangential pressure on normal pressure (Eq. (7)). In this work, the distribution of mobilized friction along the silo height was evaluated as the maximum value over time in every vertical area *i* for both filling and emptying phases.

$$Fn_i = \sum_{j=1}^{24} Fn_{i,j} \tag{3}$$

$$Ft_i = \sum_{j=1}^{24} Ft_{i,j} \tag{4}$$

$$Pn_i = \frac{Fn_i}{Ar_i} \tag{5}$$

$$Pt_i = \frac{Ft_i}{Ar_i} \tag{6}$$

$$\mu_{w,i} = \frac{Pt_i}{Pn_i} \tag{7}$$

3 Results and discussions

3.1 Effect on simulation time

Time step and particles number are the two main parameters that have a significant influence on the total computing time. The time step is fixed as 30% of Rayleigh's time, which is changing with particle radius as shown in Table 2. The volume scale factor, f_V, has been defined as the ratio between the volume of the scaled particle (V_S) and the original particle volume (V_0) (Eq. (8)). The total number of scaled particles (N_p) decreases as the volume scale factor (f_V) increases according to Eq. (9), where $N_{p,0}$ represents the number of particles generated for each silo model when using the unscaled particle. Table 3 shows particles numbers after escalation and their rates on particles number of real scale (f_R = 1.0).

Particles number has been reduced by more than 40% just by using a radius scale factor of 1.2. When f_R of 2.0 is used, the N_p reaches 12.5% of the real scale particles

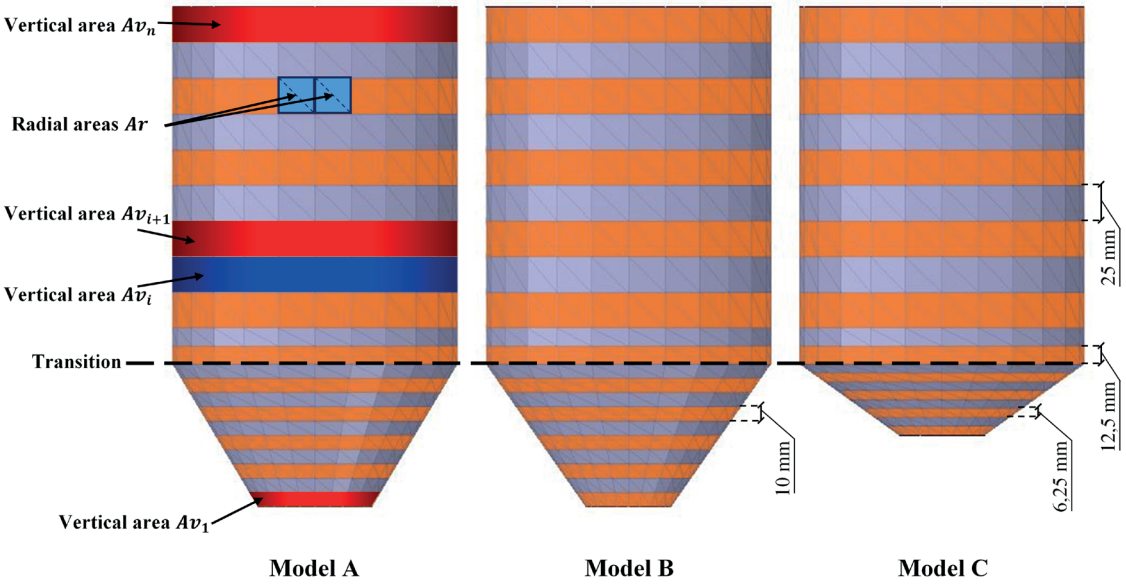

Fig. 4 Vertical divisions of silos mesh

Table 3 Particles number for different f_R and f_V

f_R	f_V	Model A		Model B		Model C	
		N_p	Rate (%)	N_p	Rate (%)	N_p	Rate (%)
1.0	1.00	235916	100	232925	100	213482	100
1.2	1.73	136567	57.89	134834	57.89	123568	57.88
1.4	2.74	86011	36.46	84928	36.46	77754	36.42
1.6	4.10	57619	24.42	56908	24.43	52136	24.42
1.8	5.83	40472	17.16	39970	17.16	36613	17.15
2.0	8.00	29505	12.51	29146	12.51	26690	12.50
2.2	10.65	22167	9.40	21892	9.40	20056	9.39
2.4	13.82	17073	7.24	16862	7.24	15450	7.24
2.6	17.58	13426	5.69	13259	5.69	12146	5.69
2.8	21.95	10752	4.56	10617	4.56	9722	4.55
3.0	27.00	8735	3.70	8632	3.71	7908	3.70

number and about 3.7% by using f_R of 3.0. The reduction of particles can be predicted by following Eq. (9), where it is valid for all three models.

$$f_V = \frac{V_s}{V_0} = f_R^3 \tag{8}$$

$$N_p = \frac{N_{p,0}}{f_V} \tag{9}$$

The simulation time is affected by particles number reduction. Fig. 5 represents the relationship between the simulation speed factor, f_S, and f_R or f_V. The factor f_S is defined as the ratio of the simulation time with f_R = 1.0, on the simulation time of other f_R, where all simulations are performed on a computing machine with CPU Intel Core i7-7700 (3.60 GHz) and 16 GB of RAM. As shown in Fig. 5(a), f_S has a cubic relationship with f_R, while, with f_V it is linear (Fig. 5(b)). The speed of simulation is increased two times by using f_R of 1.2, where the computing time of the emptying phase has reduced from around 194 hours (f_R = 1.0) to around 97 hours (f_R = 1.2). A reduction of 12 times has occurred with f_R of 2.0 (around 16 hours), and more than 43 times (around 4.5 hours) when f_R of 3.0 is used. We can deduce the formula of this relationship by using linear regression as shown in Eq. (10), with a coefficient of determination R^2 = 0.9988. This relationship is in agreement with the other researchers such as [17], who found that the computing time is decreasing by following a power law and this reduction is not only because of the particles number reduction but also due to the augmentation of the time step.

$$f_S = 1.64 \times f_V - 0.64 = 1.64 \times f_R^3 - 0.64 \tag{10}$$

3.2 Bulk density

The bulk density was calculated at the static state moment before the emptying phase, by dividing the total mass of particles inside the silo on silo volume that occupied by these particles. At the same moment, we have calculated the variation of bulk density along with silo height by using vertical partitions of 50 mm for each height. Fig. 6 represents the density of bulk material (ρ_b) inside the silo at the moment of the static state as a function of f_R. All values are roughly equal with slight augmentation from 849.5 kg/m³ for real scale until 854.9 kg/m³ for f_R of 2.0. From f_R of 2.0 to 3.0, the bulk density almost has the same value (about 854 kg/m³) except the last one with a value of 852.5 kg/m³.

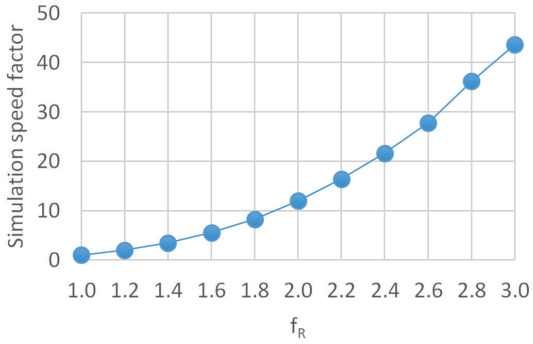

(a)

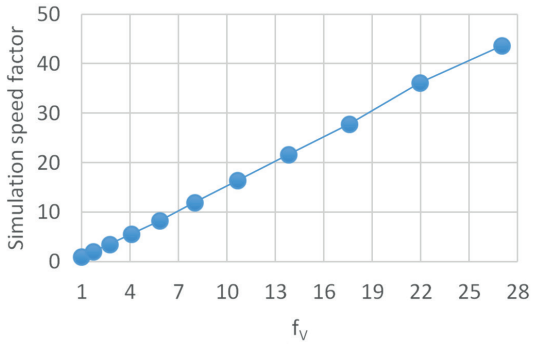

(b)

Fig. 5 Simulation speed factor as a function of f_R and f_V

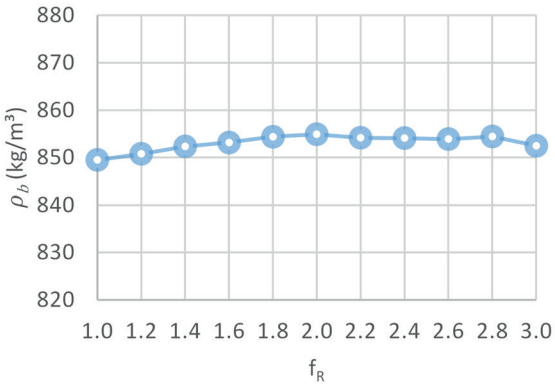

Fig. 6 Bulk density ρ_b as a function of f_R

The maximum difference of bulk density for all f_R is 5.5 kg/m³, which represents only 0.65% of the difference with respect to the reference value. On the other hand, the minimum value is 849.5 kg/m³ and the maximum is 854.9 kg/m³.

The bulk density is changing over height as shown in Fig. 7, which represents the distribution of bulk density along with silo height. This distribution is evaluated by using 5 vertical divisions of the volume for the bin of the silo. Two divisions are used for the hopper of models A and B while only one division is used for the hoper of model C. Particle upscaling has a slight effect on the distribution of density along with the silo height. The big size of particles compared to the container volume reduces the measurement precision, which appears as oscillations of values as shown in Fig. 7. This effect is similar for the three models where the only difference is the hopper size. The density value at the hopper bottom is clearly influenced by f_R, it decreases by augmenting the scale factor f_R. The small volume of the hopper near the outlet is the common thing that makes this effect appears clearly at that level of the silo. Owing to the short hopper height of model C, it has only one division to evaluate the density. Therefore, the effect of density reduction appears on the entire hopper zone. Density distribution is influenced by the distance between the center of particles that determines their position. The big distance between particles positions leads to assign some of them to a certain volume (the virtual containers that are used to calculate the density for every height), meanwhile, they have a part of them belongs to another volume. This makes the flutters appear in the curve of the density distribution over height with higher f_R. Hopper type doesn't influence the distribution of density, where the volume size comparing to particles size is the only parameter that influences the precision of calculation.

3.3 Pressures

The design of silo walls is based on extreme cases, which are the maximum possible pressures applied on the walls. Therefore, the distribution of pressures and mobilized friction of the three models are represented for the time that corresponds to the maximum values as shown in Figs. 8–10. For the filling, the represented values are obtained for the end of the case that has the extreme values. On the other hand, the beginning of the emptying is the time that corresponds to the represented values of this case. During the emptying, we have noticed that there is one case of a remarkable arching for model B with the scale factor of 3.0, and it lasted for 0.3 seconds. Otherwise, all emptying processes were stable and no arching effect was observed.

All models have the same typical curve of pressure for both cases, filling and emptying, where it grows by moving downward and it reaches the bin maximum pressure at the bottom as expected. A small reduction in pressure can be seen just above the transition before getting the peak value at the top of the hopper. This trend agrees

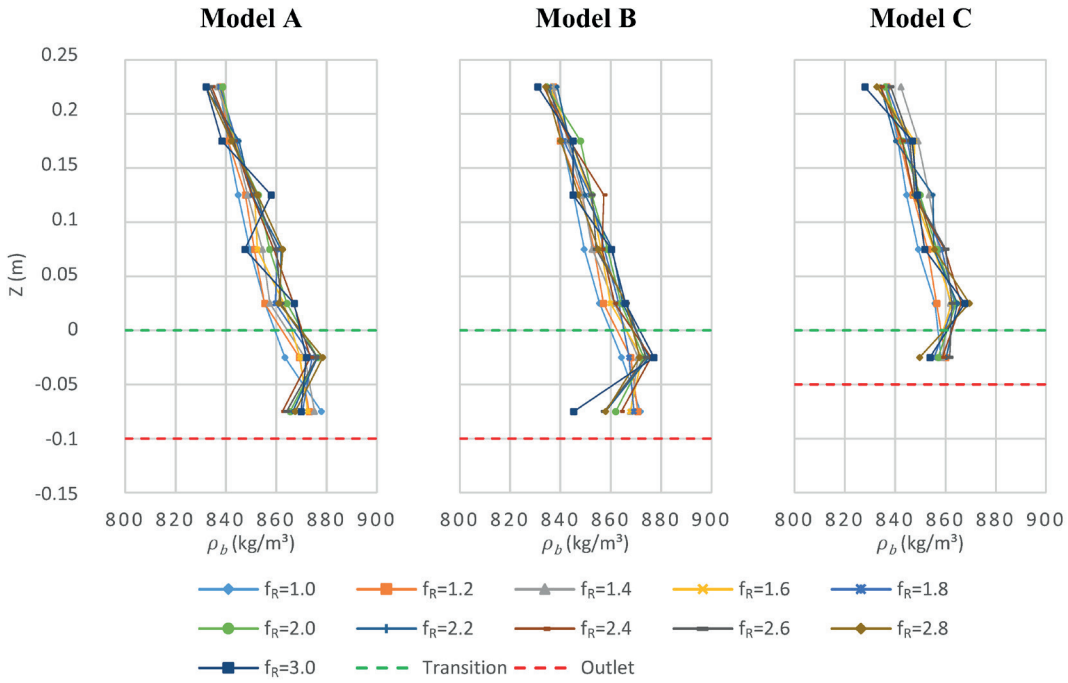

Fig. 7 Distribution of bulk density ρ_b over silo height

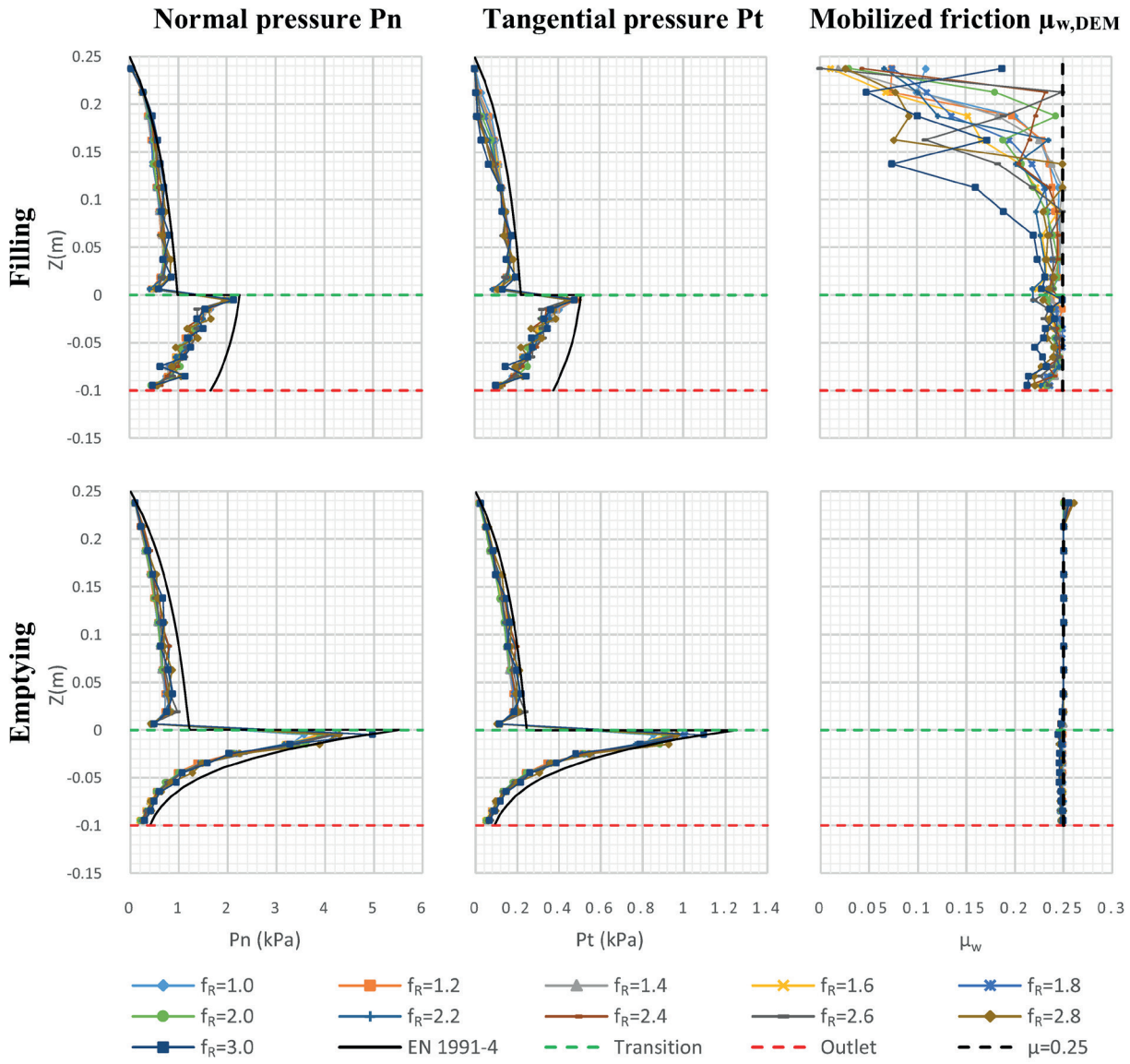

Fig. 8 Pressure distribution and mobilized friction during filling and emptying phases of model A

with simulations made by other authors [7, 11, 34], also with the experiment results [35]. The particles exerted on the inclined hopper apply an inclined reaction on the particles of the bin just above the transition. This inclined reaction is divided into two components, the vertical component that makes the vertical equilibrium, and the horizontal component (towards the center of the silo), which is against the normal pressure. By going down over the hopper wall, the pressure starts reducing until reaching the minimum value at the outlet level.

The European standard [31], EC, is represented by the black continuous line for the normal and tangential pressure of both cases, filling and emptying. EC results are slightly greater than the DEM simulation results at the bin wall, where the maximum values are 0.99 kPa and 0.22 kPa for the normal and tangential pressures, respectively of all models for the filling case. For the emptying case, the bin wall has greater maximum pressure than the filling case for all models, which are 1.21 kPa and 0.24 kPa for the normal and tangential pressures, respectively. The hopper has greater EC filling values than the simulation at the bottom, while the transition zone, which is the critical area with the peak values, has very close values to the simulation results. Hopper pressures of the emptying case are roughly equal to the simulation.

During the emptying phase, the values of pressures applied to the bin wall are slightly greater than the filling as expected [35]. On the other hand, the hopper experiences a significant increase compared to the filling. The particle upscaling almost has no effect on pressure values.

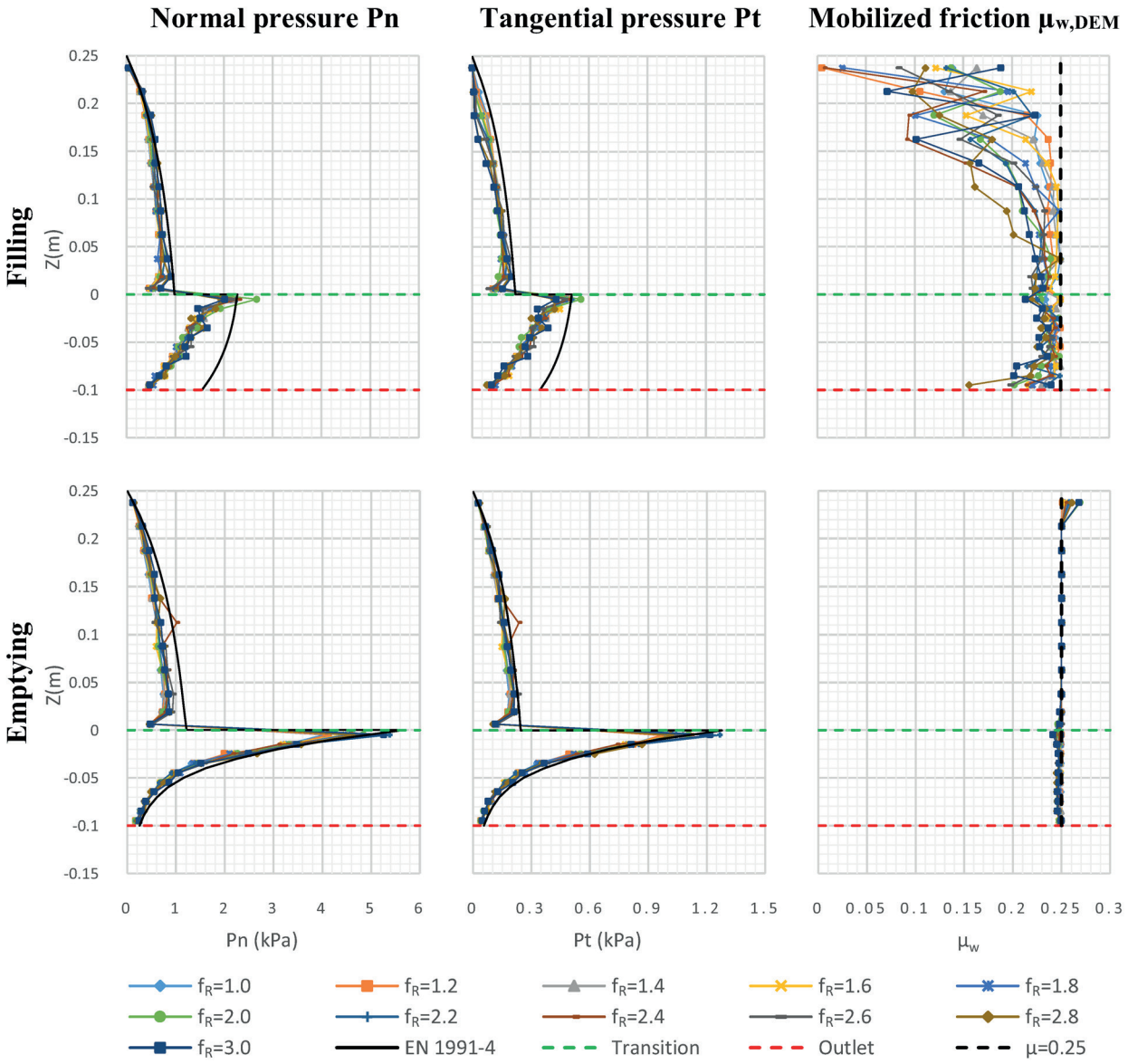

Fig. 9 Pressure distribution and mobilized friction during filling and emptying phases of model B

However, some slight changes have been noticed, where the curves become more flutter by augmenting the scale factor, especially during the filling phase. The hopper curve has more and larger flutters than the curve of the bin. This refers to the mesh size comparing to the size of the particle, where the bin mesh is coarser than the mesh of the hopper (Fig. 4). In addition, the tangential pressure of the filling case has zero values on a certain height at the top of the silo bin, and that height expands as the f_R increases. These two phenomena are not noticeable during the emptying phase because of the movement of particles downward, which makes a smooth contact with the wall and a smooth pressure curve.

All variations of emptying peak values of all models with all f_R values are lower than the EC values, except for model C with f_R = 2.60 that is slightly higher than the EC value. The normal pressure has peak values of 2.26 kPa, 2.27 kPa, and 2.34 kPa for the filling case of models A, B, and C, respectively, and 5.53 kPa, 5.68 kPa, and 6.24 kPa for the emptying case. Tangential pressures of filling are 0.51 kPa, for models A and B, and 0.42 kPa for model C, while the emptying case has values of 1.24 kPa, 1.28 kPa, and 1.13 kPa for models A, B and C, respectively.

Fig. 11 represents the peak values at the transition zone as a function of f_R for the three models. Fig. 11(a)–(b) are obtained by using the fine mesh represented in Fig. 4

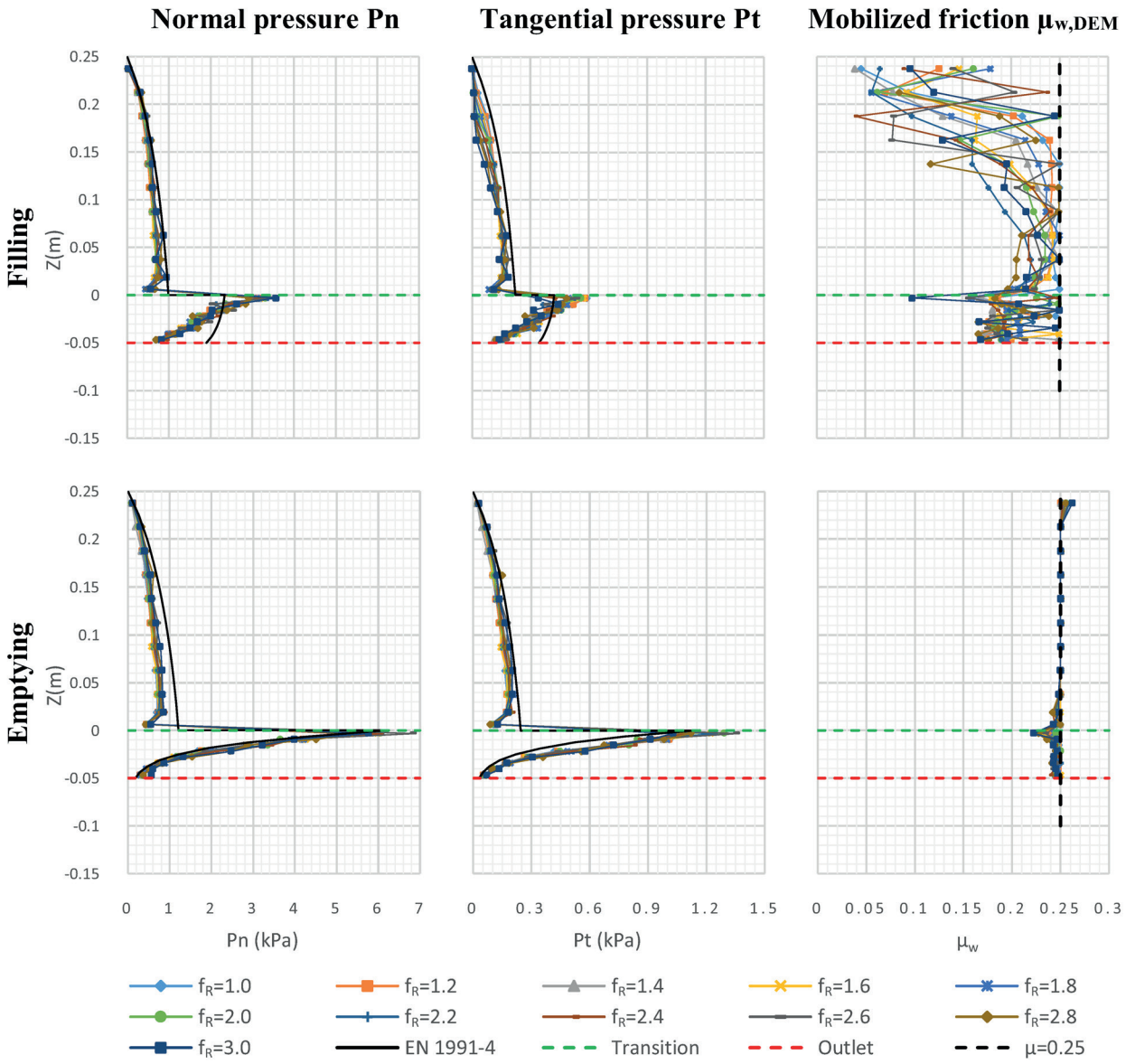

Fig. 10 Pressure distribution and mobilized friction during filling and emptying phases of model C

for filling (Fig. 11(a)) and emptying (Fig. 11(b)), while Fig. 11(c) and Fig. 11(d) represent the results obtained for filling and emptying respectively by using a coarse mesh-size at the transition zone (the mesh height increased two times). The transition peak value is an expected trend as widely observed experimentally and numerically [35, 36] and according to [37], the particles movement downward and the sudden change of their direction from the vertical to the hopper direction are the main reason for this peak pressure right after the transition zone.

For the emptying phase, the peak value is changing randomly when the f_R value changes as shown in Fig. 11(b). The peak value of normal pressure is varying from 3.57 kPa to 4.98 kPa for model A (maximum increase of 39.50% comparing to the value of f_R = 1.0). For model B, it is between 4.03 kPa and 5.38 kPa (33.50%), and for model C, it changes from 5.10 kPa to 6.85 kPa (34.31%). The tangential pressure peak value is between 0.85 kPa and 1.1 kPa for model A, between 1 kPa and 1.25 kPa for model B, and for model C, it is varying from 1 kPa to 1.35 kPa. The filling case has more stable and steady peak values than the emptying (Fig. 11(a)), especially for model A. Model B has an outlier for f_R = 2.0 with a 21.92% increase compared with the reference value. Model C has two extremes peak values corresponding to f_R = 2.8 (-9.91%) and f_R = 3.0 (10.53%), respectively. The variation of the peak value returns to the fine mesh size of the hopper, where model C has the smallest hopper mesh among the three models,

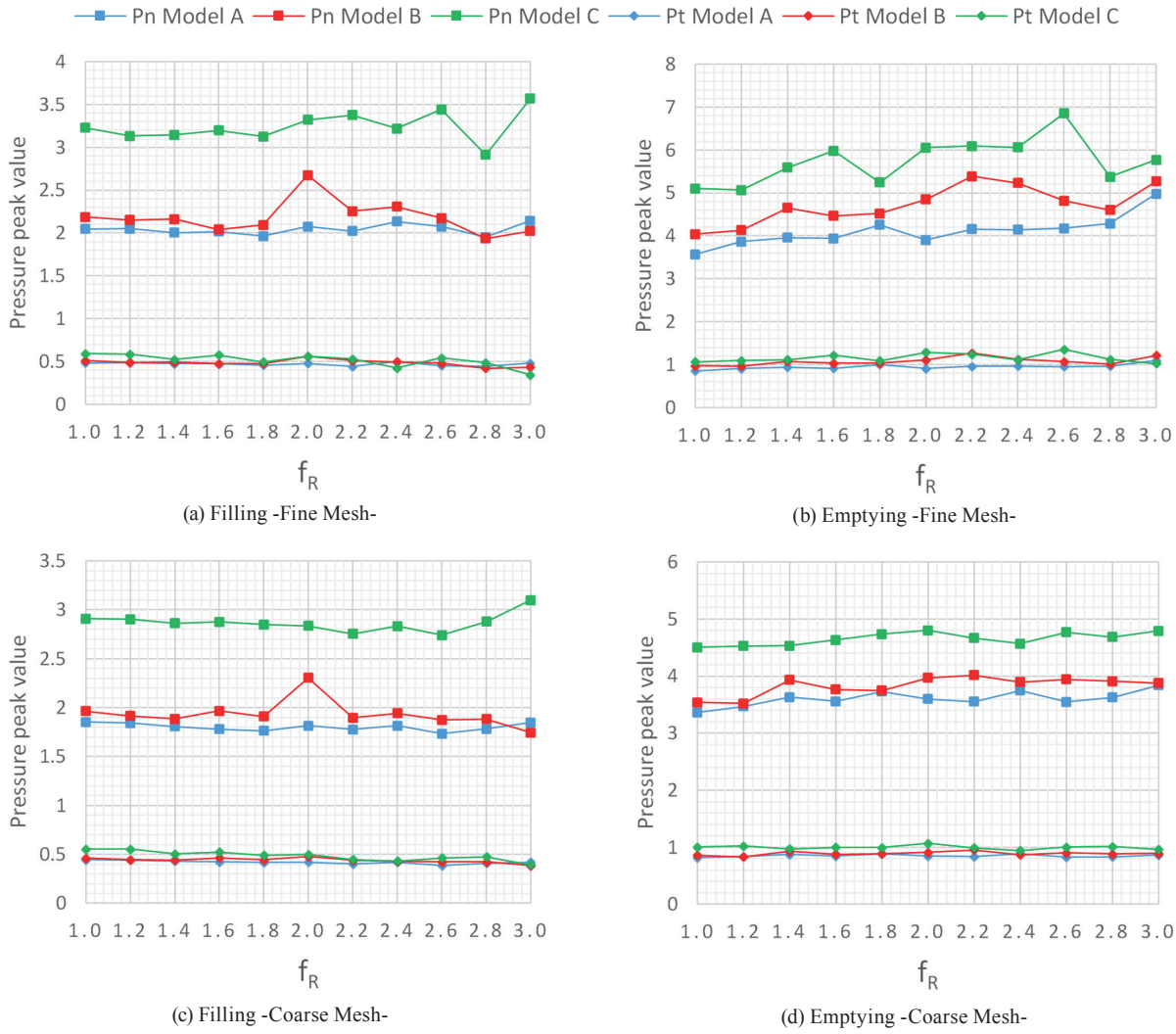

Fig. 11 The variation of pressures peak value during filling with a fine mesh (a), emptying with a fine mesh (b), filling with a coarse mesh (c), and emptying with a coarse mesh (d) as a function of f_R

which corresponds to the biggest variation range of the peak value with 1.8 kPa for the emptying normal pressure and 0.35 kPa for the emptying tangential pressure. On the other side, the variation range of the peak value for both models A and B is 1.4 kPa for the emptying normal pressure and 0.25 kPa for the emptying tangential pressure. Depending on the particle shape, the contact between the particle and the wall would be in limited points, in our case, two points maximum, unlike the real case where the particle is not rigid and the contact with the walls would be in a surface. The big particle size may lead to making irregular distribution of contacts with the fine mesh areas. The pressure is the value of the force divided by the area to which this force is applied on. The irregular distribution of forces makes differences in pressure value that assigned to the consecutive areas, it appears as flutters on pressures curves. To avoid this effect, it should be taken into consideration the mesh sizing with particle upscaling. By increasing the mesh size to double (Fig. 11(c)–(d)), the influence of particle upscaling on the peak pressure at the transition zone is almost disappeared. The curve of peak pressure is almost steady with the variation of the scaling factor and it appears obviously by comparing the curve of the fine mesh (Fig. 11(b)) with the curve of the coarse mesh (Fig. 11(d)).

The mobilized friction of all models steady at the value of 0.25 for the emptying case as the expected value, where it was used as the coefficient of static friction between the steel silo wall and the wheat particles. By upscaling the particle, the mobilized friction at the hopper area experiences a slight reduction. However, it stayed between 0.24 and 0.25 except for the transition zone of model C, where the mobilized friction at that point is reduced to reach 0.22

for some f_R values. The curve of the filling case is different compared to the emptying, however, the values stayed less than or equal to 0.25. We can notice that all mobilized friction values of the filling case decrease upward and vice versa with downward. The hopper area experienced more stable values and closer to the expected, mostly limited in the range of 0.2 to 0.25 except for model C, where the range is between 0.15 and 0.25 for most values. However, this trend is also observed by other authors [7, 34]. This phenomenon returns to the low vertical pressure where the mobilized friction is not fully generated. The weight of wheat applies more vertical pressure downwards, which explains the values that are close to the expected at the hopper. By increasing the f_R value, mobilized friction is decreasing for the filling case and more flutters appear in its curves. This behavior could be due to the big size of particles, which reduces the contact number between them and silo walls. This reduction of contact leads to reduce the evaluation precision of values and it can be solved by increasing the mesh size to expand the contact area. The emptying case did not experience this behavior because of the motion of particles, which creates a smooth contact during the emptying process.

Fig. 12, Fig. 13, and Fig. 14 show the color map representation of the normal pressure, tangential pressure, and the mobilized friction for filling and emptying for models A, B, and C, respectively. The represented values are calculated for each time step as the ratio between the normal pressure, tangential pressure, or mobilized friction of every vertical area and the maximum value over time of the same area corresponding to these values. Thus, the scale ranges from 0 to 1, where pure white is the minimum value (0), and pure black is the maximum value (1). The vertical axis represents the coordinates of the vertical areas measured on meters (Z). Positive values of Z correspond to locations at the bin wall, while negative values of Z refer to the hopper. Finally, the horizontal axis represents the percentage of computing time considered (T), where 0% corresponds to the start of the simulation and 100% refers to the end of the simulation, both for filling and discharge processes.

We can see that there is a smooth change of values from one moment to another for all results of all models, where the evolution of these values over time is almost the same. The triangle shape of all color map representations refers to the graduate filling and emptying process, where the

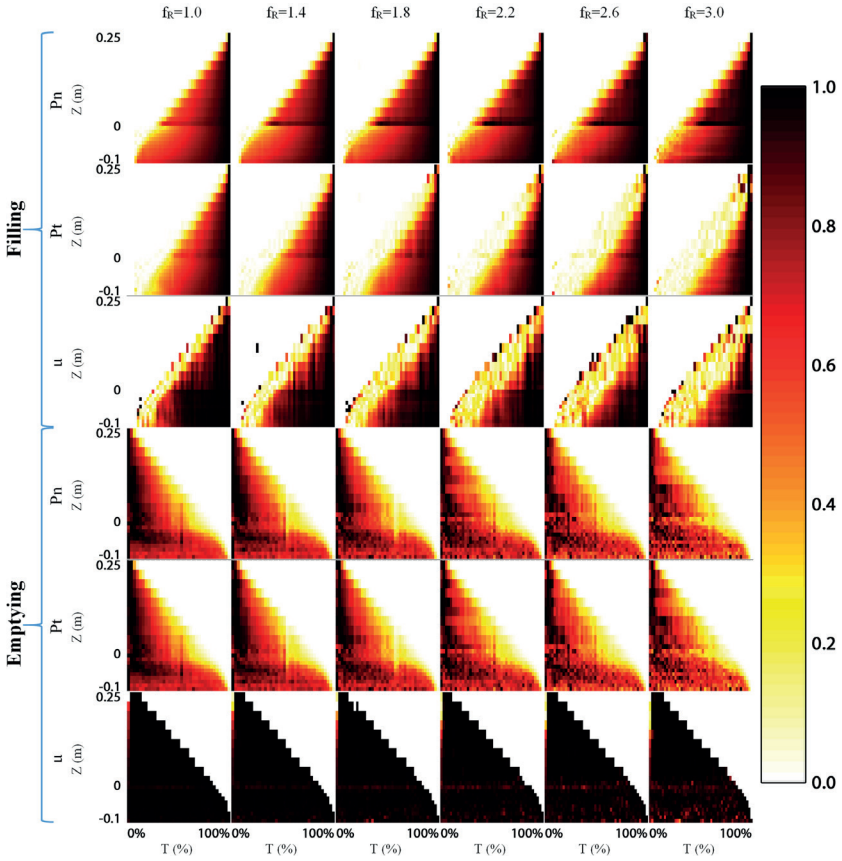

Fig. 12 Color map representation of the normal pressure, tangential pressure, and the mobilized friction for filling and emptying of model A

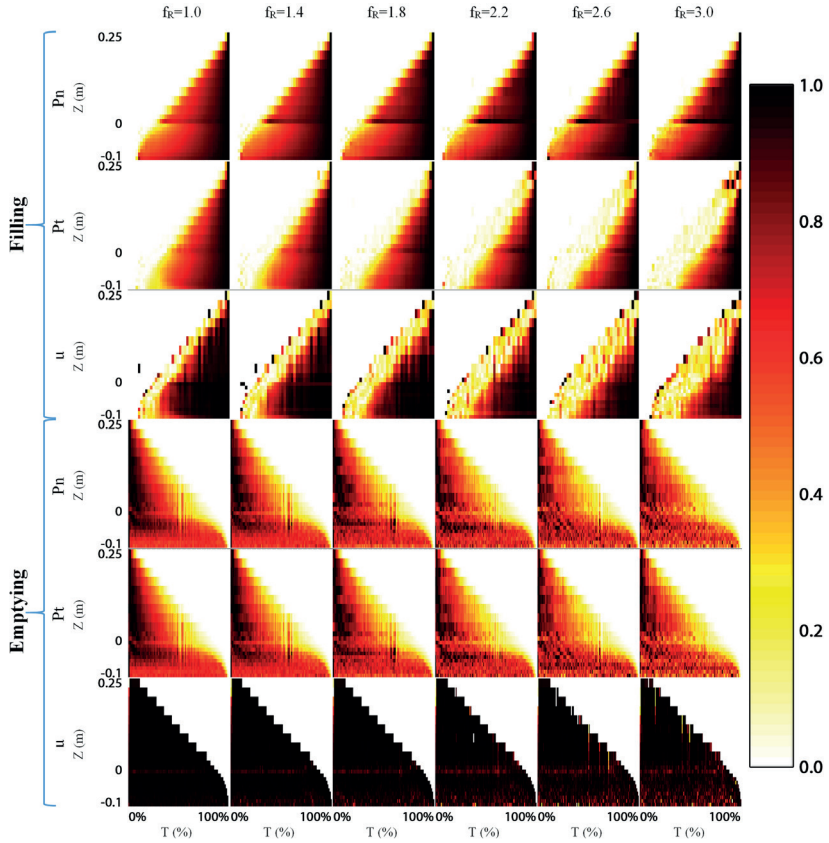

Fig. 13 Color map representation of the normal pressure, tangential pressure, and the mobilized friction for filling and emptying of model B

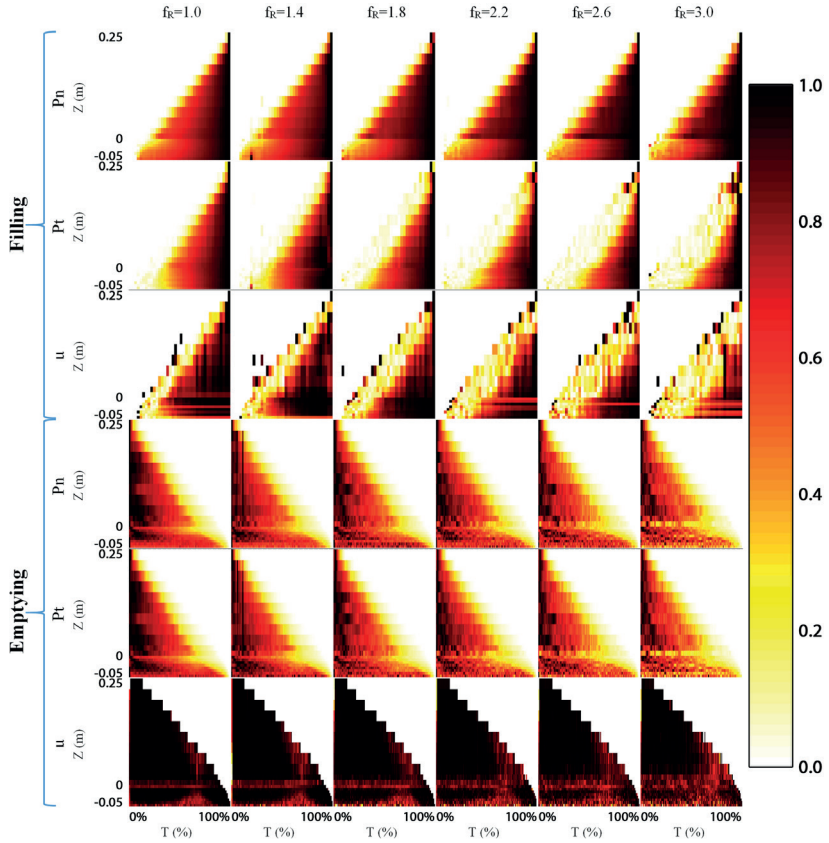

Fig. 14 Color map representation of the normal pressure, tangential pressure, and the mobilized friction for filling and emptying of model C

contact between the wall and particles starts from the bottom to the top progressively for the filling, and vice versa with the emptying.

The filling case values start to increase gradually from the moment of the first contact of the wall with particles until the end of the filling that represents the moment of the maximum value over time. The mobilized friction is also increasing gradually during the filling until reaches the expected value at the end. Again, the low vertical pressure at the beginning of the filling (due to the less mass) prevents the mobilized friction from being fully generated. All representations of emptying pressures start with the maximum values and they are reducing with time until the end of the phase. There is a small effect of f_R on the evolution of values over time and it is similar for all models. The normal pressure of the filling phase is increasing faster over time when f_R increases, while the tangential pressure is increasing slower. As a result, the mobilized friction also follows the same behavior of tangential pressure. We can notice this effect clearly at the zone just above the transition, where the three models have higher values at the beginning of the filling with higher f_R. This means that filling pressure reaches its maximum earlier at this zone with particle upscaling. This trend is related to the fall of particles during progressive filling where the upscaled particle has a higher impact force than the unscaled as noticed by some authors [23, 24]. At the beginning of the filling, particles fall from the maximum height, and as filling progresses, this height reduces progressively until the end of the filling. Therefore, the impact force effect has the maximum influence at the beginning of the filling and this effect is reducing as well by the filling progress. This effect does not appear in the unscaled models or the models with a small scaling factor because the impact force of the small particle is not noticeable. In our simulations, the relatively short silos do not lead to generating an impact force higher than the mass weight of the full filled silo even with the scaling factor of 3.0. Hence, the maximum values are obtained at the end of the filling regardless of the particle scale. However, a scaling factor higher than 3.0 may cause a higher maximum pressure with the use of the progressive filling method with these models. The fall height should be reduced relating to the scale factor to avoid this effect. Or we can reduce the generation rate to keep the same impact force as the unscaled model.

For the emptying phase, the effect appears as a reduction in the smoothness of values evolution with the augmentation of f_R, it can be seen as noise in the represented images. However, this reduction doesn't influence on results values comparing to the other f_R for the same corresponding time. Unlike the filling case, mobilized friction results for the emptying have steady values over time. With higher f_R, a small noise can be observed in the hopper zone, it appears as a result of the normal and tangential pressure noises. This effect can be seen clearly with model C, where it has some values lower than expected at the transition zone. In addition, the augmentation of f_R makes this noise spread more to occupy a slightly bigger area over the hopper. This effect returns to the inaccurate evaluation of normal and tangential pressures with upscaling technique and that due to the non-regular distribution of contact between particles and silo walls. The bigger particle applies a greater force concentrated on one fine mesh area instead of distributing it over many mesh areas (in the case of the small particles). At the same time, the other mesh areas around the contacted area will be contactless with the big particles and this will cause the noise to appear. This effect can be seen over height (transition and hopper zone) and over time (at the end of the emptying phase). Model C has the most inclined hopper (the highest apex half-angle β) and it is associated with the funnel flow. With this flow type, the lateral particles (those situated near the hopper walls) have a very slow movement and this causes a slightly similar effect to the filling when the mobilized friction is not fully generated. For this, the noise effect has more influence on this model especially at the end of the emptying when the vertical pressure is reduced. Also, the particle upscaling influences the discharge flow by slowing down the velocity of the particles, and this will increase the effect as clearly observed with the upscaled models. However, it doesn't make a remarkable influence on the final results.

4 Conclusions

This paper is studying the effect of the particle size on pressures obtained from DEM simulation of a cylindrical silo with a hopper during the filling and the emptying. Three silo models have been used with different outlet sizes and hopper inclinations. The effect of particle upscaling on pressures and granular flow is studied by taking into consideration the different silo types.

The total number of particles is extremely reduced with particle upscaling by following a relationship based on power law. Thus, the computing time is following the same behavior.

The bulk density does not change with particle escalation but the distribution over height is slightly changed due to numerical measurement precision.

Maximum pressures remain almost the same with particle upscaling. However, geometry mesh sizing must be chosen carefully to avoid random variation of pressures and to obtain a more stable curve, especially for the transition peak value.

The upscaled particles have a greater impact force during the progressive filling and this leads to generating a slightly greater pressure at the beginning of the filling. In addition, the high impact force makes the particles well compacted and this may lead to generate a greater normal pressure in some cases, such as the big silos with higher particle generators.

References

[1] EDEM "User Guide", DEM Solutions Ltd., Edinburgh, Scotland, UK, 2018.

[2] Gallego, E., Fuentes, J. M., Wiącek, J., Villar, J. R., Ayuga, F. "DEM analysis of the flow and friction of spherical particles in steel silos with corrugated walls", Powder Technology, 355, pp. 425–437, 2019. https://doi.org/10.1016/j.powtec.2019.07.072

[3] Golshan, S., Esgandari, B., Zarghami, R., Blais, B., Saleh, K. "Experimental and DEM studies of velocity profiles and residence time distribution of non-spherical particles in silos", Powder Technology, 373, pp. 510–521, 2020. https://doi.org/10.1016/j.powtec.2020.06.093

[4] Hlosta, J., Jezerská, L., Rozbroj, J., Žurovec, D., Nečas, J., Zegzulka, J. "DEM Investigation of the Influence of Particulate Properties and Operating Conditions on the Mixing Process in Rotary Drums: Part 1 – Determination of the DEM Parameters and Calibration Process", Processes, 8(2), Article number: 222, 2020. https://doi.org/10.3390/pr8020222

[5] Kumar, R., Patel, C. M., Jana, A. K., Gopireddy, S. R. "Prediction of hopper discharge rate using combined discrete element method and artificial neural network", Advanced Powder Technology, 29(11), pp. 2822–2834, 2018. https://doi.org/10.1016/j.apt.2018.08.002

[6] Najafi-Sani, M. A., Mansourpour, Z. "Application of a new method for experimental validation of polydispersed DEM simulation of silo discharge", Advanced Powder Technology, 31(11), pp. 4457–4469, 2020. https://doi.org/10.1016/j.apt.2020.09.021

[7] González-Montellano, C., Gallego, E., Ramírez-Gómez, Á., Ayuga, F. "Three dimensional discrete element models for simulating the filling and emptying of silos: Analysis of numerical results", Computers & Chemical Engineering, 40, pp. 22–32, 2012. https://doi.org/10.1016/j.compchemeng.2012.02.007

[8] Tian, T., Su, J., Zhan, J., Geng, S., Xu, G., Liu, X. "Discrete and continuum modeling of granular flow in silo discharge", Particuology, 36, pp. 127–138, 2018. https://doi.org/10.1016/j.partic.2017.04.001

[9] Coetzee, C. J., Els, D. N. J. "Calibration of discrete element parameters and the modelling of silo discharge and bucket filling", Computers and Electronics in Agriculture, 65(2), pp. 198–212, 2009. https://doi.org/10.1016/j.compag.2008.10.002

[10] Ketterhagen, W. R., Curtis, J. S., Wassgren, C. R., Hancock, B. C. "Predicting the flow mode from hoppers using the discrete element method", Powder Technology, 195(1), pp. 1–10, 2009. https://doi.org/10.1016/j.powtec.2009.05.002

[11] Markauskas, D., Ramírez-Gómez, Á., Kačianauskas, R., Zdancevičius, E., "Maize grain shape approaches for DEM modelling", Computers and Electronics in Agriculture, 118, pp. 247–258, 2015. https://doi.org/10.1016/j.compag.2015.09.004

[12] Chung, Y.-C., Ooi, J. Y. "A study of influence of gravity on bulk behaviour of particulate solid", Particuology, 6(6), pp. 467–474, 2008. https://doi.org/10.1016/j.partic.2008.07.017

[13] Feng, Y. T., Owen, D. R. J. "Discrete element modelling of large scale particle systems – I: exact scaling laws", Computational Particle Mechanics, 1, pp. 159–168, 2014. https://doi.org/10.1007/s40571-014-0010-y

[14] Janda, A., Ooi, J. Y. "DEM modeling of cone penetration and unconfined compression in cohesive solids", Powder Technology, 293, pp. 60–68, 2016. https://doi.org/10.1016/j.powtec.2015.05.034

[15] Smith, W., Melanz, D., Senatore, C., Iagnemma, K., Peng, H. "Comparison of discrete element method and traditional modeling methods for steady-state wheel-terrain interaction of small vehicles", Journal of Terramechanics, 56, pp. 61–75, 2014. https://doi.org/10.1016/j.jterra.2014.08.004

[16] Ciantia, M. O., Arroyo, M., Butlanska, J., Gens, A. "DEM modelling of cone penetration tests in a double-porosity crushable granular material", Computers and Geotechnics, 73, pp. 109–127, 2016. https://doi.org/10.1016/j.compgeo.2015.12.001

[17] Coetzee, C. J. "Particle upscaling: Calibration and validation of the discrete element method", Powder Technology, 344, pp. 487–503, 2019. https://doi.org/10.1016/j.powtec.2018.12.022

[18] Lommen, S., Mohajeri, M., Lodewijks, G., Schott, D. "DEM particle upscaling for large-scale bulk handling equipment and material interaction", Powder Technology, 352, pp. 273–282, 2019. https://doi.org/10.1016/j.powtec.2019.04.034

[19] Mohajeri, M. J., Helmons, R. L. J., van Rhee, C., Schott, D. L. "A hybrid particle-geometric scaling approach for elasto-plastic adhesive DEM contact models", Powder Technology, 369, pp. 72–87, 2020. https://doi.org/10.1016/j.powtec.2020.05.012

[20] Nasato, D. S., Goniva, C., Pirker, S., Kloss, C. "Coarse Graining for Large-scale DEM Simulations of Particle Flow – An Investigation on Contact and Cohesion Models", Procedia Engineering, 102, pp. 1484–1490, 2015. https://doi.org/10.1016/j.proeng.2015.01.282

[21] Queteschiner, D., Lichtenegger, T., Pirker, S., Schneiderbauer, S. "Multi-level coarse-grain model of the DEM", Powder Technology, 338, pp. 614–624, 2018.
https://doi.org/10.1016/j.powtec.2018.07.033

[22] Roessler, T., Katterfeld, A. "Scaling of the angle of repose test and its influence on the calibration of DEM parameters using upscaled particles", Powder Technology, 330, pp. 58–66, 2018.
https://doi.org/10.1016/j.powtec.2018.01.044

[23] Grima, A. P., Wypych, P. W. "Investigation into calibration of discrete element model parameters for scale-up and validation of particle–structure interactions under impact conditions", Powder Technology, 212(1), pp. 198–209, 2011.
https://doi.org/10.1016/j.powtec.2011.05.017

[24] Xie, L., Zhong, W., Zhang, H., Yu, A., Qian, Y., Situ, Y. "Wear process during granular flow transportation in conveyor transfer", Powder Technology, 288, pp. 65–75, 2016.
https://doi.org/10.1016/j.powtec.2015.10.043

[25] Achmus, M., Abdel-Rahman, K. "The influence of "up-scaling" on the results of particle method calculations of non-cohesive soils", In: Konietzky, H. (ed.) Numerical Modeling in Micromechanics via Particle Methods, Routledge, London, UK, 2003, pp. 183–187.
https://doi.org/10.1201/9780203745335-24

[26] Bierwisch, C., Kraft, T., Riedel, H., Moseler, M. "Three-dimensional discrete element models for the granular statics and dynamics of powders in cavity filling", Journal of the Mechanics and Physics of Solids, 57(1), pp. 10–31, 2009.
https://doi.org/10.1016/j.jmps.2008.10.006

[27] Weinhart, T., Labra, C., Luding, S., Ooi, J. Y. "Influence of coarse-graining parameters on the analysis of DEM simulations of silo flow", Powder Technology, 293, pp. 138–148, 2016.
https://doi.org/10.1016/j.powtec.2015.11.052

[28] Cundall, P. A., Strack, O. D. L. "A discrete numerical model for granular assemblies", Géotechnique, 29(1), pp. 47–65, 1979.
https://doi.org/10.1680/geot.1979.29.1.47

[29] Noh, G., Bathe, K.-J. "An explicit time integration scheme for the analysis of wave propagations", Computers & Structures, 129, pp. 178–193, 2013.
https://doi.org/10.1016/j.compstruc.2013.06.007

[30] Horabik, J., Molenda, M., "Parameters and contact models for DEM simulations of agricultural granular materials: A review", Biosystems Engineering, 147, pp. 206–225, 2016.
https://doi.org/10.1016/j.biosystemseng.2016.02.017

[31] CEN "EN 1991-4, Eurocode 1: Actions on Structures - Part 4: Silos and Tanks", European Committee for Standardization, Brussels, Belgium, 2006.

[32] Safranyik, F. "Gravitational and vibrational discharge of silos", PhD Thesis, Szent István University, 2016.
https://doi.org/10.14751/SZIE.2017.007

[33] Keppler, I., Kocsis, L., Oldal, I., Farkas, I., Csatar, A. "Grain velocity distribution in a mixed flow dryer", Advanced Powder Technology, 23(6), pp. 824–832, 2012.
https://doi.org/10.1016/j.apt.2011.11.003

[34] González-Montellano, C., Ramírez, A., Fuentes, J. M., Ayuga, F. "Numerical effects derived from en masse filling of agricultural silos in DEM simulations", Computers and Electronics in Agriculture, 81, pp. 113–123, 2012.
https://doi.org/10.1016/j.compag.2011.11.013

[35] Ramírez, A., Nielsen, J., Ayuga, F. "Pressure measurements in steel silos with eccentric hoppers", Powder Technology, 201(1), pp. 7–20, 2010.
https://doi.org/10.1016/j.powtec.2010.02.027

[36] Gallego, E., Ruiz, A., Aguado, P. J. "Simulation of silo filling and discharge using ANSYS and comparison with experimental data", Computers and Electronics in Agriculture, 118, pp. 281–289, 2015.
https://doi.org/10.1016/j.compag.2015.09.014

[37] Jenike, A. W., Johanson, J. R. "Bin Loads", Journal of the Structural Division, 94(4), pp. 1011–1041, 1968.
https://doi.org/10.1061/JSDEAG.0001928